Measurement of the $B^{\pm}$ production asymmetry and the CP asymmetry in $B^{\pm} \to J/\psi K^{\pm}$ decays

LHCb Collaboration ; Bernet, R ; Müller, K ; Serra, N ; Steinkamp, O ; Straumann, U ; Vollhardt, A ; et al

Abstract: The $B^{\pm}$ meson production asymmetry in pp collisions is measured using $B^{+} \to \overline{D}^{0}\pi^{+}$ decays. The data were recorded by the LHCb experiment during Run 1 of the LHC at center-of-mass energies of $\sqrt{s} = 7$ and 8 TeV. The production asymmetries, integrated over transverse momenta in the range $2 < p_T < 30 GeV/c$, and rapidities in the range $2.1 < y < 4.5$ are measured to be $\mathcal{A}_{prod}(B^{+}, \sqrt{s} = 7TeV) = (0.41 \pm 0.49 \pm 0.10) \times 10^{2}$, $\mathcal{A}_{prod}(B^{+}, \sqrt{s} = 8TeV) = (0.53 \pm 0.31 \pm 0.10) \times 10^{2}$, where the first uncertainties are statistical and the second are systematic. These production asymmetries are used to correct the raw asymmetries of $B^{+} \to J/\psi K^{\pm}$ decays, thus allowing a measurement of the CP asymmetry, $\mathcal{A}_{CP}(B^{+} \to J/\psi K^{\pm}) = (0.09 \pm 0.27 \pm 0.07) \times 10^{2}$.

DOI: https://doi.org/10.1103/PhysRevD.95.052005

Originally published at:
LHCb Collaboration; Bernet, R; Müller, K; Serra, N; Steinkamp, O; Straumann, U; Vollhardt, A; et al (2017). Measurement of the $B^{\pm}$ production asymmetry and the CP asymmetry in $B^{\pm} \to J/\psi K^{\pm}$ decays. Physical review D, D95(5):052005.
DOI: https://doi.org/10.1103/PhysRevD.95.052005

PHYSICAL REVIEW D **95,** 052005 (2017)

Measurement of the $B^{\pm}$ production asymmetry and the CP asymmetry in $B^{\pm} \to J/\psi K^{\pm}$ decays

R. Aaij *et al.*[*]
(LHCb Collaboration)

(Received 20 January 2017; published 22 March 2017)

The $B^{\pm}$ meson production asymmetry in pp collisions is measured using $B^+ \to \bar{D}^0\pi^+$ decays. The data were recorded by the LHCb experiment during Run 1 of the LHC at center-of-mass energies of $\sqrt{s} = 7$ and 8 TeV. The production asymmetries, integrated over transverse momenta in the range $2 < p_{\mathrm{T}} < 30$ GeV/c, and rapidities in the range $2.1 < y < 4.5$ are measured to be $\mathcal{A}_{\mathrm{prod}}(B^+, \sqrt{s} = 7\ \mathrm{TeV}) = (-0.41 \pm 0.49 \pm 0.10) \times 10^{-2}$, $\mathcal{A}_{\mathrm{prod}}(B^+, \sqrt{s} = 8\ \mathrm{TeV}) = (-0.53 \pm 0.31 \pm 0.10) \times 10^{-2}$, where the first uncertainties are statistical and the second are systematic. These production asymmetries are used to correct the raw asymmetries of $B^+ \to J/\psi K^+$ decays, thus allowing a measurement of the CP asymmetry, $\mathcal{A}_{CP}(B^+ \to J/\psi K^+) = (0.09 \pm 0.27 \pm 0.07) \times 10^{-2}$.

DOI: 10.1103/PhysRevD.95.052005

I. INTRODUCTION

One of the primary goals of the LHCb experiment is to search for effects of physics beyond the Standard Model through measurements of CP-violating asymmetries in beauty- and charm-hadron decays. A challenge for such measurements in pp collisions is that the heavy flavor production rates differ between particles and antiparticles. These production asymmetries cannot be precisely predicted since they arise in the nonperturbative b or c quark hadronization process [1–3]. The effects of production asymmetries cancel in measurements of the difference between CP asymmetries of two different decays of the same hadron species.

The CP asymmetries of B^+ meson decay rates[1] are often measured relative to that of the decay $B^+ \to J/\psi K^+$. The leading tree-level diagram for this decay, shown in Fig. 1 (left), is color suppressed, and the total decay amplitude may receive a sizeable contribution from the gluonic loop diagram shown in Fig. 1 (right). Therefore, the $B^+ \to J/\psi K^+$ decay can in principle exhibit a CP asymmetry due to the interference between these amplitudes. The current world average value of the CP asymmetry is $\mathcal{A}_{CP}(B^+ \to J/\psi K^+) = (0.3 \pm 0.6)\%$ [4], and the uncertainty represents a limitation in many B^+ meson CP asymmetry measurements that use this channel as a reference.

This analysis exploits the decay $B^+ \to \bar{D}^0\pi^+$, which is dominated by a Cabibbo- and color-favored tree-level amplitude and is therefore expected to have a CP asymmetry with a smaller value and uncertainty than for the $B^+ \to J/\psi K^+$ mode. The $B^+ \to \bar{D}^0\pi^+$ decay mode is used to measure the production asymmetry between the cross sections for B^- and B^+ mesons, defined as

$$\mathcal{A}_{\mathrm{prod}}(B^+) \equiv \frac{\sigma(B^-) - \sigma(B^+)}{\sigma(B^-) + \sigma(B^+)}. \tag{1}$$

Since the production asymmetry is expected to be a function of the kinematics, the measurement is performed in nine bins of B^+ transverse momentum, p_{T}, and rapidity, y, within the fiducial region $2 < p_{\mathrm{T}} < 30$ GeV/c and $2.1 < y < 4.5$. Measurements are performed on two data sets corresponding to integrated luminosities of 1 and 2 fb^{-1}, recorded at center-of-mass energies of 7 and 8 TeV in 2011 and 2012, respectively. These measurements complement the existing LHCb studies of heavy flavor production asymmetries [5–8]. A combined analysis of $B^+ \to \bar{D}^0\pi^+$ and $B^+ \to J/\psi K^+$ decays allows a measurement of the CP asymmetry in the latter mode. The raw charge asymmetry for a flavor-specific decay to the final state f ($\bar{f}$) accessible in decays of B^- (B^+) mesons is defined as

$$\mathcal{A}_{\mathrm{raw}}(B^+ \to \bar{f}) \equiv \frac{N(B^- \to f) - N(B^+ \to \bar{f})}{N(B^- \to f) + N(B^+ \to \bar{f})}. \tag{2}$$

For the two decay modes under study, the asymmetries are well approximated by

[*]Full author list given at the end of the article.

[1]The inclusion of charge-conjugate processes is implied throughout, except in the discussion of asymmetries.

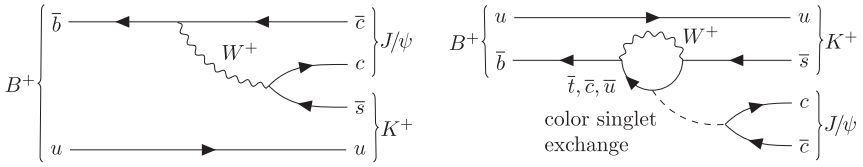

FIG. 1. Tree and loop (penguin) diagrams for the $B^+ \to J/\psi K^+$ decay.

$$\begin{aligned}\mathcal{A}_{\rm raw}(B^+ \to \bar{D}^0\pi^+) &= \mathcal{A}_{\rm prod}(B^+) + \mathcal{A}_{\rm det}(\bar{D}^0\pi^+) \\ &\quad + \mathcal{A}_{CP}(B^+ \to \bar{D}^0\pi^+), \\ \mathcal{A}_{\rm raw}(B^+ \to J/\psi K^+) &= \mathcal{A}_{\rm prod}(B^+) + \mathcal{A}_{\rm det}(J/\psi K^+) \\ &\quad + \mathcal{A}_{CP}(B^+ \to J/\psi K^+), \end{aligned} \tag{3}$$

where $\mathcal{A}_{\rm det}$ is the detector-induced asymmetry resulting from differences in the detection efficiencies between particles and antiparticles. All contributions to $\mathcal{A}_{\rm det}$ are measured on independent control samples from the same data set. The high correlation of $\mathcal{A}_{\rm det}$ between the two decay modes implies a partial cancellation in their difference. This cancellation and the low level of CP violation in the $B^+ \to \bar{D}^0\pi^+$ decay mode enable a precise measurement of $\mathcal{A}_{CP}(B^+ \to J/\psi K^+)$.

II. LHCB DETECTOR

The LHCb detector [9,10] is a single-arm forward spectrometer covering the pseudorapidity range $2 < \eta < 5$, designed for the study of particles containing b or c quarks. The detector includes a high-precision tracking system consisting of a silicon-strip vertex detector surrounding the pp interaction region, a large-area silicon-strip detector located upstream of a dipole magnet with a bending power of about 4 Tm, and three stations of silicon-strip detectors and straw drift tubes placed downstream of the magnet. Data samples corresponding to roughly equal integrated luminosities were recorded with configurations in which the magnetic field was pointing vertically upward and downward. This largely canceled any charge asymmetries in the reconstruction efficiency for charged particles. The tracking system provides a measurement of momentum, p, of charged particles with a relative uncertainty that varies from 0.5% at low momentum to 1.0% at 200 GeV/c. The minimum distance of a track to a primary vertex (PV), the impact parameter (IP), is measured with a resolution of $(15 + 29/p_{\rm T})$ μm, where $p_{\rm T}$ is the component of the momentum transverse to the beam, in GeV/c. Different types of charged hadrons are distinguished using information from two ring-imaging Cherenkov detectors. Muons are identified by a system composed of alternating layers of iron and multiwire proportional chambers. The online event selection is performed by a trigger [11], which consists of a hardware stage, based on information from the calorimeter and muon systems, followed by a two-stage software trigger, which applies a full event reconstruction. This analysis makes use of inclusive dimuon and beauty selections at the software trigger stages.

III. SELECTION OF $B^+ \to \bar{D}^0\pi^+$ DECAYS

The selection of signal candidate $B^+ \to \bar{D}^0\pi^+$ decays closely follows a recent LHCb analysis involving the same decay channel [12]. Events are considered for the analysis if they contain a track with large enough $p_{\rm T}$ and IP to satisfy the requirements of the first stage of the software trigger. An inclusive beauty selection is applied at the second stage of the software trigger. Candidate $\bar{D}^0 \to K^+\pi^-(\bar{D}^0 \to K^+\pi^+\pi^-\pi^-)$ decays are constructed from the intersection of two (four) tracks that satisfy appropriate kaon or pion particle identification (PID) criteria and that have a large $p_{\rm T}$ and significant IP with respect to all primary vertices. These candidates must have a mass within ± 25 MeV/c^2 of the $\bar{D}^0$ mass [4]. Each $\bar{D}^0$ candidate is combined with a high-$p_{\rm T}$ track that is identified as a pion to create a displaced vertex that is consistent with the decay of a B^+ meson. The B^+ candidates are required to have a mass within the range 5079–5899 MeV/c^2. To reduce to a negligible level the uncertainty related to L0 trigger asymmetries, it is explicitly required that a positive L0 trigger decision was caused by a particle that is distinct from any of the final-state particles that compose the signal candidate. This requirement is independent of whether or not the signal candidate itself also caused a positive L0 trigger decision and is therefore referred to as triggered independently of signal (TIS) [11].

For both the two- and four-body $\bar{D}^0$-mode selections, a pair of boosted decision tree (BDT) discriminators [13], implementing the gradient boost algorithm [14], is used to achieve further background suppression. The first of these BDTs is trained to reject candidates with fake $\bar{D}^0$ decays, and the second is trained to reject backgrounds with real $\bar{D}^0$ decays. The BDTs are trained using simulated $B^+ \to \bar{D}^0\pi^+$ signal decays and a sample of decays from data with masses in the range 5900–7200 MeV/c^2 to model the combinatorial background in the nominal mass range. For the training of the first BDT, a background sample is provided by candidates with $\bar{D}^0$ masses that differ by more than ± 30 MeV/c^2 from the known $\bar{D}^0$ mass. The second BDT is trained using a background sample of candidates with $\bar{D}^0$ masses within ± 25 MeV/c^2 of the known $\bar{D}^0$ mass. A loose cut on the classifier response of the first BDT is

applied prior to training the second one. The inputs into the BDTs include properties of each particle (p, p_{T}, and the IP significance) and additional properties of the B and D^0 composite particles (decay time, flight distance, decay vertex quality, radial distance between the decay vertex and the PV, and the angle between the reconstructed momentum vector and the line connecting the production and decay vertex). A further input into the BDTs is an isolation variable,

$$I_{p_{\mathrm{T}}} = \frac{p_{\mathrm{T}}(B^{\pm}) - \Sigma p_{\mathrm{T}}}{p_{\mathrm{T}}(B^{\pm}) + \Sigma p_{\mathrm{T}}}, \tag{4}$$

for which the sum is taken over tracks that are not part of the signal candidate but fall within a cone of half-angle $\Delta R < 1.5$ rad, where $(\Delta R)^2 = (\Delta\theta)^2 + (\Delta\phi)^2$, and $\Delta\theta$ and $\Delta\phi$ are the differences in the polar and azimuthal angles of each track with respect to the B^+ candidate direction. Tracks are only considered in the isolation cone if they are associated, by the smallest IP, to the same primary vertex as the signal candidate. Signal decays are expected to have larger values of $I_{p_{\mathrm{T}}}$ than background.

The cut on the second BDT response is optimized by minimizing the expected uncertainty on the asymmetry between the yields of $B^- \to D^0\pi^-$ and $B^+ \to \bar{D}^0\pi^+$. No PID information is used in the BDT training, but the purity of the sample is further improved by requiring all kaon and pion candidates to satisfy PID criteria. Events containing more than one $B^+ \to \bar{D}^0\pi^+$ candidate amount to less than 1%, and in these cases, the candidate with the highest-quality B^+ decay vertex is selected.

The raw asymmetries between the yields of $B^- \to D^0\pi^-$ and $B^+ \to \bar{D}^0\pi^+$ decays are determined by binned maximum likelihood fits to the mass distributions of selected B^- and B^+ candidates, treating the two- and four-body $\bar{D}^0$ modes separately. The fit function is built from a signal component and three background components. A sum of two Gaussian functions with asymmetric power-law tails and an additional Gaussian function are combined to model $B^+ \to \bar{D}^0\pi^+$ decays [12]. Misidentified $B^+ \to \bar{D}^0K^+$ decays have a distribution that is below the signal peak with a tail that extends to lower masses. They are modeled by the sum of two Gaussian functions with asymmetric power-law tail components. Partially reconstructed decays with an additional particle from a D^* or ρ meson decay form a background at masses lower than that of the signal peak. This component is described by a combination of analytical functions with shapes that depend on the spin parity of the missing particle, following the method described in Ref. [12]. A linear function is adequate to describe the combinatorial background distribution. The yield of misidentified $B^+ \to \bar{D}^0K^+$ decays is constrained with an independent control sample of these decays, combined with the calibrated particle identification efficiencies and misidentification rates [15]. With the exception of the tail parameters, which are fixed to values obtained from simulation, all parameters are allowed to vary in the fit.

Figure 2 shows the fits to the mass distributions in the bin with $4.5 < p_{\mathrm{T}} < 9.5$ GeV/c and $2.10 < y < 2.85$. The subsequent analysis is based on separate fits for the nine kinematic bins and two center-of-mass energies. The signal yields for each of the nine kinematic bins are listed in Table I. The p_{T} and y intervals of each bin are defined in the second and third columns. The yields sum over $B^{\pm}$ meson charges and center-of-mass energies. Integrated over the fiducial acceptance, $2 < p_{\mathrm{T}} < 30$ GeV/c and $2.1 < y < 4.5$, the fits return signal yields of around 2.3×10^5 decays for the $\bar{D}^0 \to K^+\pi^-$ mode and around 1.3×10^5 decays for the $\bar{D}^0 \to K^+\pi^+\pi^-\pi^-$ mode.

IV. SELECTION OF $B^+ \to J/\psi K^+$ DECAYS

The selection of $B^+ \to J/\psi K^+$ decays with $J/\psi \to \mu^+\mu^-$ is based on events in which a muon or a generic track, with large p_{T} and IP significance, satisfies the requirements of the first-stage software trigger. Events must be selected based on a dimuon signature by the second-level software trigger. Candidate $J/\psi \to \mu^+\mu^-$ decays are reconstructed from high-p_{T} muon candidates with large IPs with respect to all PVs. A mass interval of 3057–3127 MeV/c^2 is imposed on the J/ψ candidates. These candidates are combined with a high-p_{T} identified kaon with a significant IP with respect to all PVs, where the J/ψ candidate invariant mass is constrained to its known value in the combination. The L0 trigger TIS requirement is applied in the same way as for the $\bar{D}^0\pi^+$ selection. A single BDT classifier is used to improve the purity of the $B^+ \to J/\psi K^+$ sample. This classifier is trained on a similar set of variables as that for the $B^+ \to \bar{D}^0\pi^+$ selection and exhibits very similar performance in terms of signal efficiency and background rejection. Events containing more than one $B^+ \to J/\psi K^+$ candidate amount to less than 1%, and in these cases, the candidate with the highest-quality B^+ decay vertex is selected.

A simultaneous fit of the mass distributions across the kinematic bins is performed, where the same value of $\mathcal{A}_{CP}(B^+ \to J/\psi K^+)$ is assumed for all bins. The signal peak is described using a Gaussian function with an additional asymmetric power-law tail component. The mean of the Gaussian is constrained to be the same in all kinematic bins, while its width and the tail parameters are allowed to vary between bins. A small background from misidentified $B^+ \to J/\psi\pi^+$ decays is described by a similar function, with fixed shape parameters taken from simulation. The yield of this contribution is allowed to vary in each kinematic bin, but a single raw asymmetry is shared between all bins. The contribution from random particle combinations is described by a linear function. The yield of this component and the slope parameter are allowed to vary

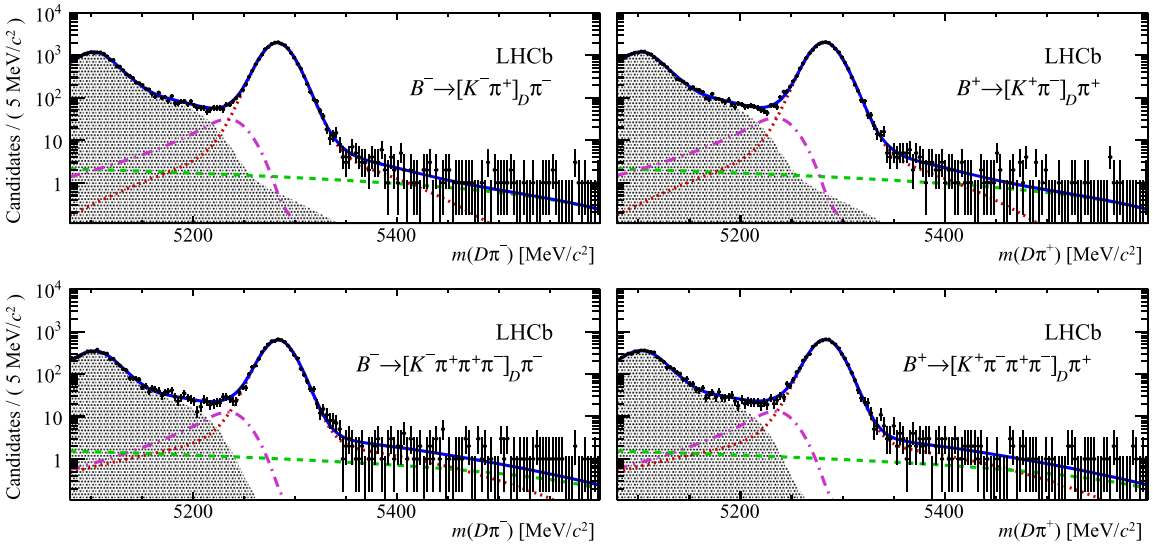

FIG. 2. Mass distributions of selected (top) $B^\pm \to [K^\pm\pi^\mp]_D\pi^\pm$ and (bottom) $B^\pm \to [K^\pm\pi^\pm\pi^\mp\pi^\mp]_D\pi^\pm$ candidates in the bin with $4.5 < p_T < 9.5$ GeV/c and $2.10 < y < 2.85$. These distributions sum over the two center-of-mass energies. B^- candidates are displayed on the left, and B^+ candidates are on the right. The red dotted lines indicate the contribution from $B^\pm \to D\pi^\pm$ decays. The purple dashed-dotted lines indicate the contribution from misidentified $B^\pm \to DK^\pm$ decays. The gray shaded regions at low values of reconstructed mass indicate the contribution from various partially reconstructed B decays, and the green dashed lines indicate the combinatorial background. The total fit function is shown by the blue solid lines. The fit in other kinematic bins is similar, aside from the specific signal and background component yields.

in each kinematic bin. The yield is also fitted separately for each $B^\pm$ charge.

Integrated over the full fiducial acceptance, a signal yield of about 2.3×10^5 events is measured. Table I lists the yields of each signal decay mode in each of the kinematic bins summing over the two center-of-mass energies. An example of the fit in the bin with $4.5 < p_T < 9.5$ GeV/c and $2.10 < y < 2.85$ is displayed in Fig. 3.

V. MEASUREMENT OF THE B^+ PRODUCTION ASYMMETRY

The B^+ production asymmetry is determined in the nine bins of p_T and y according to

$$\mathcal{A}_{\rm prod}(B^+) = \mathcal{A}^{D\pi}_{\rm raw} - \mathcal{A}^{D\pi}_{CP} - \mathcal{A}^{K\pi}_{\rm det} - \mathcal{A}^{\pi}_{\rm det} - \mathcal{A}^{\rm PID}_{\rm det} - \mathcal{A}^{\rm TIS}_{\rm det}, \tag{5}$$

where $\mathcal{A}^{D\pi}_{\rm raw}$ and $\mathcal{A}^{D\pi}_{CP}$ are the raw charge asymmetry and CP asymmetry in the $B^+ \to \bar{D}^0\pi^+$ decay, respectively. The four $\mathcal{A}_{\rm det}$ terms correct for detector-induced asymmetries and will be described in the following. All terms other than $\mathcal{A}^{D\pi}_{CP}$ are evaluated separately for the four disjoint data sets corresponding to the two center-of-mass energies and the two magnet polarities. An average of the $\mathcal{A}^{D\pi}_{\rm raw}$ values for the two $\bar{D}^0$ decay modes is computed with weights that are chosen to minimize the uncertainty. The same weights are used to compute averages over the two $\bar{D}^0$ decay modes for

TABLE I. The p_T and y intervals for each kinematic bin and the corresponding signal yields in each of the B^+ decay modes, summing over the two center-of-mass energies.

Bin	p_T (GeV/c)	y	$B^+ \to \bar{D}^0\pi^+$, $\bar{D}^0 \to K^+\pi^-$	$\bar{D}^0 \to K^+\pi^-\pi^+\pi^-$	$B^+ \to J/\psi K^+$, $J/\psi \to \mu^+\mu^-$
1	2.0–4.5	2.10–2.85	13604 ± 118	1549 ± 42	17319 ± 194
2	2.0–4.5	2.85–3.3	18587 ± 145	4022 ± 66	26038 ± 229
3	2.0–4.5	3.3–4.5	19946 ± 151	6347 ± 87	31110 ± 260
4	4.5–9.5	2.10–2.85	44470 ± 219	14209 ± 131	34939 ± 231
5	4.5–9.5	2.85–3.3	47597 ± 240	23895 ± 163	36682 ± 230
6	4.5–9.5	3.3–4.5	31137 ± 200	24014 ± 170	31345 ± 212
7	9.5–30	2.10–2.85	33516 ± 195	23378 ± 167	25174 ± 189
8	9.5–30	2.85–3.3	20176 ± 159	20332 ± 151	15110 ± 136
9	9.5–30	3.3–4.5	4767 ± 73	8832 ± 97	8602 ± 191
Integrated			233390 ± 537	126350 ± 393	226319 ± 632

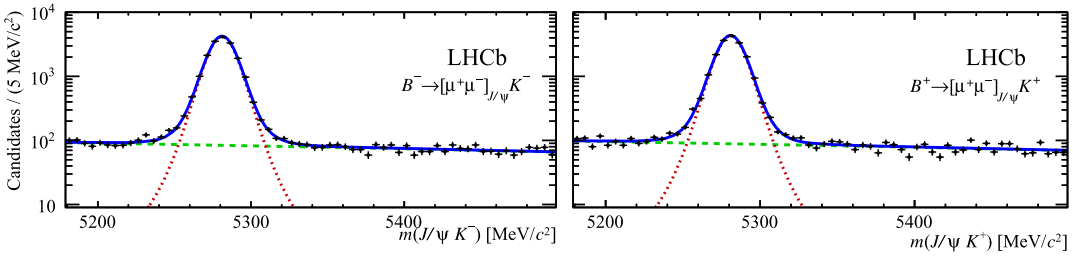

FIG. 3. Mass distribution of selected $B^{\pm} \to J/\psi K^{\pm}$ candidates in the bin with $4.5 < p_{\mathrm{T}} < 9.5$ GeV/c and $2.10 < y < 2.85$. These distributions sum over the two center-of-mass energies. B^- candidates are displayed on the left, and B^+ candidates are on the right. The signal components are displayed as red dotted lines, while the background from combinatorial events is shown by the green dashed lines. The fit in other kinematic bins is similar, aside from the specific signal and background component yields.

all other terms in Eq. (5) apart from $\mathcal{A}_{\mathrm{det}}^{\mathrm{TIS}}$, which is independent of the $\bar{D}^0$ decay. Tables II and III list the values of the first five terms in Eq. (5) for the 7 and 8 TeV data sets, respectively. The overall detection asymmetry has two main contributions. The first arises because K^- mesons have a larger nuclear interaction cross section than K^+ mesons. This means that more K^- mesons than K^+ mesons interact inelastically with the detector material before they leave enough hits to be reconstructed in the tracking stations. The resulting K^-–K^+ detection asymmetry is around 10^{-2}. The second cause of asymmetry is the different trajectories of positively and negatively charged particles, which therefore have different sensitivities to misalignments and inhomogeneities of the detector. This source contributes to all detection asymmetry terms. It is partially cancelled when averaging measurements over data recorded with the dipole magnet in the two polarities.

The $\bar{D}^0$ detection asymmetry, $\mathcal{A}_{\mathrm{det}}^{K\pi}$, is measured using samples of D^- mesons that are produced in the primary pp interactions and decay to the $K^+\pi^-\pi^-$ and $K_S^0\pi^-$ final

TABLE II. A summary of the terms that enter the production asymmetry determination [Eq. (5)] in the 7 TeV data set. The p_{T} and y intervals of each bin are provided in Table I. The L0 trigger asymmetry $\mathcal{A}_{\mathrm{det}}^{\mathrm{TIS}}$ is omitted from this table since it is assumed to be independent of the B^+ kinematics. All uncertainties are statistical.

Bin	$\mathcal{A}_{\mathrm{raw}}^{D\pi}$ ($\times 10^{-2}$)	$\mathcal{A}_{CP}^{D\pi}$ ($\times 10^{-2}$)	$\mathcal{A}_{\mathrm{det}}^{K\pi}$ ($\times 10^{-2}$)	$\mathcal{A}_{\mathrm{det}}^{\pi}$ ($\times 10^{-2}$)	$\mathcal{A}_{\mathrm{det}}^{\mathrm{PID}}$ ($\times 10^{-2}$)
1	-1.1 ± 1.5	$+0.08 \pm 0.05$	-1.39 ± 0.22	-0.04 ± 0.13	-0.066 ± 0.006
2	-1.5 ± 1.3	$+0.08 \pm 0.05$	-1.18 ± 0.15	-0.05 ± 0.08	$+0.017 \pm 0.017$
3	-1.7 ± 1.1	$+0.07 \pm 0.05$	-1.19 ± 0.16	-0.04 ± 0.09	$+0.077 \pm 0.007$
4	-1.1 ± 0.8	$+0.07 \pm 0.05$	-1.23 ± 0.21	$+0.03 \pm 0.11$	-0.0875 ± 0.0021
5	-1.6 ± 0.7	$+0.07 \pm 0.04$	-1.03 ± 0.13	$+0.03 \pm 0.08$	-0.049 ± 0.004
6	-1.5 ± 0.8	$+0.06 \pm 0.04$	-1.10 ± 0.13	-0.02 ± 0.08	$+0.2092 \pm 0.0033$
7	-0.7 ± 0.8	$+0.06 \pm 0.04$	-0.84 ± 0.20	$+0.04 \pm 0.13$	-0.0606 ± 0.0026
8	-2.6 ± 0.9	$+0.05 \pm 0.04$	-0.65 ± 0.12	$+0.05 \pm 0.12$	$+0.0645 \pm 0.0022$
9	-0.2 ± 1.6	$+0.04 \pm 0.04$	-1.07 ± 0.11	$+0.06 \pm 0.12$	$+0.3951 \pm 0.0032$

TABLE III. A summary of the terms that enter the production asymmetry determination [Eq. (5)] in the 8 TeV data set. The L0 trigger asymmetry $\mathcal{A}_{\mathrm{det}}^{\mathrm{TIS}}$ is omitted from this table since it is assumed to be independent of the B^+ kinematics. All uncertainties are statistical.

Bin	$\mathcal{A}_{\mathrm{raw}}^{D\pi}$ ($\times 10^{-2}$)	$\mathcal{A}_{CP}^{D\pi}$ ($\times 10^{-2}$)	$\mathcal{A}_{\mathrm{det}}^{K\pi}$ ($\times 10^{-2}$)	$\mathcal{A}_{\mathrm{det}}^{\pi}$ ($\times 10^{-2}$)	$\mathcal{A}_{\mathrm{det}}^{\mathrm{PID}}$ ($\times 10^{-2}$)
1	-0.7 ± 1.0	$+0.08 \pm 0.05$	-1.16 ± 0.13	-0.17 ± 0.09	$+0.059 \pm 0.004$
2	-1.2 ± 0.9	$+0.07 \pm 0.05$	-1.08 ± 0.09	-0.10 ± 0.06	$+0.0855 \pm 0.0029$
3	-2.8 ± 0.8	$+0.07 \pm 0.05$	-0.93 ± 0.10	-0.07 ± 0.06	$+0.0659 \pm 0.0026$
4	-1.3 ± 0.5	$+0.07 \pm 0.05$	-1.07 ± 0.12	-0.10 ± 0.07	-0.0144 ± 0.0008
5	-1.7 ± 0.4	$+0.07 \pm 0.04$	-0.99 ± 0.08	-0.11 ± 0.05	$+0.0963 \pm 0.0013$
6	-1.2 ± 0.5	$+0.06 \pm 0.04$	-0.79 ± 0.08	-0.06 ± 0.06	$+0.1323 \pm 0.0024$
7	-1.0 ± 0.5	$+0.06 \pm 0.04$	-0.93 ± 0.11	-0.02 ± 0.08	$+0.0120 \pm 0.0012$
8	-1.0 ± 0.6	$+0.05 \pm 0.04$	-0.78 ± 0.07	-0.14 ± 0.08	$+0.0581 \pm 0.0029$
9	-1.8 ± 1.0	$+0.04 \pm 0.04$	-0.56 ± 0.07	-0.10 ± 0.08	$+0.0914 \pm 0.0017$

states. The K^0_S mesons are reconstructed in their decay to $\pi^+\pi^-$. Within a small phase-space region in terms of the D^- decay products, it is assumed that the detection asymmetry for a $K^+\pi^-$ pair can be determined using

$$\mathcal{A}^{K\pi}_{\rm det} = \mathcal{A}_{\rm raw}(D^- \to K^+\pi^-\pi^-) - \mathcal{A}_{\rm raw}(D^- \to K^0_S\pi^-), \quad (6)$$

with a small correction for the effects of CP violation in $K^0 - \bar{K}^0$ mixing and the different material interactions of K^0 and $\bar{K}^0$. For each of the $D^- \to K^+\pi^-\pi^-$ candidates, one of the two π^- mesons is randomly labelled as being *matched* to the $B^+ \to \bar{D}^0\pi^+$ signal. A weight is assigned to each $D^- \to K^+\pi^-\pi^-$ candidate such that the kinematic distributions of the K^+ and the matched π^- agree with those from the signal $\bar{D}^0$ decays. For the $\bar{D}^0 \to K^+\pi^+\pi^-\pi^-$ sample, the procedure is repeated for each of the two possible pions with opposite charge to the kaon, averaging over the two. Each $D^- \to K^0_S\pi^-$ candidate is assigned a weight, such that the π^- kinematic distributions agree with those of the *unmatched* π^- in the weighted $D^- \to K^+\pi^-\pi^-$ sample, and the D^- kinematic distributions are equalized between the two D^- decay modes. This ensures cancellation of the D^- production asymmetry and means that any detection asymmetry associated with the unmatched π^- is cancelled with a corresponding asymmetry affecting the $D^- \to K^0_S\pi^-$ sample. This weighting procedure is performed for each of the nine B^+ kinematic bins. The raw asymmetries that enter Eq. (6) are determined by fitting the weighted mass spectra for the four combinations of $D^\pm$ decay modes and charges.

Using a detailed description of the LHCb detector and cross section measurements from fixed target experiments [4], the nuclear interaction contribution to the pion asymmetry is estimated to be negligibly small. The tracking asymmetry can therefore be assumed to be the same for pions and muons. The π^+ tracking asymmetry, $\mathcal{A}^{\pi}_{\rm det}$, is therefore inferred from that of muons measured using a sample of $J/\psi \to \mu^+\mu^-$ decays in which one of the muons is reconstructed without requiring hits in all tracking stations [16]. Weights are assigned to the J/ψ candidates such that the kinematic distributions of this muon match those of the π^- in the $B^+ \to \bar{D}^0\pi^+$ sample.

The PID requirements on the $B^+ \to \bar{D}^0\pi^+$ decays can introduce asymmetries. Corrections are determined using a control sample of $D^{*+} \to D^0\pi^+$ decays, with $D^0 \to K^-\pi^+$, in which no PID requirements are imposed on the K^- or π^+ from the D^0 decay. The asymmetry associated with PID requirements on the $\bar{D}^0$ decays is partially accounted for in the $\mathcal{A}^{K\pi}_{\rm det}$ correction, since PID requirements are imposed on the final-state kaons and pions in the D^- control samples. The requirements are tighter in these control samples, and so a residual correction must still be applied. The sum of this correction, and a corresponding correction for the PID requirement on the π^+ from the $D^{*+} \to D^0\pi^+$ decays, is denoted $\mathcal{A}^{\rm PID}_{\rm det}$.

The asymmetry associated with the TIS trigger efficiency, $\mathcal{A}^{\rm TIS}_{\rm det}$, is determined using a sample of b-hadron decays to the final state $\bar{D}^0\mu^+\nu_\mu X$ with $\bar{D}^0 \to K^+\pi^-$. An unbiased probe of the TIS trigger efficiency is provided by the subset of these in which the muon prompted a positive decision by the L0 muon trigger. The corresponding asymmetries do not exhibit any kinematic dependence, and so a single correction is determined for each center-of-mass energy and is applied to all kinematic bins. The measured $\mathcal{A}^{\rm TIS}_{\rm det}$ values are $(+0.16 \pm 0.16) \times 10^{-2}$ and $(+0.02 \pm 0.10) \times 10^{-2}$ for the 7 and 8 TeV data sets, respectively.

The CP asymmetry, $\mathcal{A}^{D\pi}_{CP}$, is estimated from measurements of the angle γ of the unitarity triangle of the Cabibbo-Kobayashi-Maskawa matrix [17,18] and the hadronic parameters of $B^+ \to \bar{D}^0\pi^+$ decays [19]. Different values are obtained for the $\bar{D}^0 \to K^+\pi^-$ and $\bar{D}^0 \to K^+\pi^-\pi^+\pi^-$ decay modes due to the smaller coherence factor from the competing hadronic resonances in the four-body mode. The asymmetries are

$$\mathcal{A}^{D\pi}_{CP}(K^-\pi^+) = (0.09^{+0.05}_{-0.04}) \times 10^{-2},$$
$$\mathcal{A}^{D\pi}_{CP}(K^-\pi^+\pi^-\pi^+) = (0.00^{+0.05}_{-0.02}) \times 10^{-2},$$

with a 55% correlation between the uncertainties on these two quantities. The $\mathcal{A}^{D\pi}_{CP}$ values reported in Tables II and III are averaged over the two- and four-body modes. These values vary between the kinematic bins due to the different weights of the two- and four-body modes.

Several sources of systematic uncertainty arise in the determination of the production asymmetries. Their contributions are listed in Table IV. Variations in the weighting procedures that are used to determine $\mathcal{A}^{K\pi}_{\rm det}$ and $\mathcal{A}^{\pi}_{\rm det}$ yield uncertainties of 0.07×10^{-2} and 0.04×10^{-2}, respectively. An uncertainty of 0.04×10^{-2} is assigned to a possible pion nuclear interaction asymmetry that is not accounted for in the tracking efficiency measurements with muons from J/ψ decays. Finally, the $\mathcal{A}^{D\pi}_{CP}$ uncertainties are included in the total systematic uncertainty, which is taken to be correlated between the kinematic bins.

TABLE IV. Systematic uncertainties on the $\mathcal{A}_{\rm prod}(B^+)$ measurement. The $\mathcal{A}^{D\pi}_{CP}$ uncertainty varies between the kinematic bins, and the range is indicated. All systematic uncertainties are considered to be correlated between kinematic bins.

Source	Size ($\times 10^{-2}$)
$\mathcal{A}^{K\pi}_{\rm det}$ method	± 0.07
$\mathcal{A}^{\pi}_{\rm det}$ method	± 0.04
Pion nuclear interactions	± 0.04
$\mathcal{A}^{D\pi}_{CP}$	$\pm(0.04 - 0.05)$

TABLE V. The measured $\mathcal{A}_{\rm prod}$ values for each kinematic bin and integrated over the full kinematic acceptance, $2 < p_{\rm T} < 30$ GeV/c and $2.1 < y < 4.5$. The integrated values sum over the asymmetries in each bin, weighted by the values, w, in the second and fourth columns for the two center-of-mass energies. The first uncertainty is the statistical uncertainty on $\mathcal{A}^{D\pi}_{\rm raw}$ and is uncorrelated between the kinematic bins. The second uncertainty is the statistical uncertainty on the detection asymmetry corrections and is taken to be correlated between the kinematic bins. The third uncertainty is purely systematic and is assumed to be correlated between bins.

Bin	w(7 TeV)	$\mathcal{A}_{\rm prod}(B^+, 7\ {\rm TeV})$ $(\times 10^{-2})$	w(8 TeV)	$\mathcal{A}_{\rm prod}(B^+, 8\ {\rm TeV})$ $(\times 10^{-2})$
1	0.182	$+0.12 \pm 1.54 \pm 0.30 \pm 0.10$	0.174	$+0.42 \pm 0.96 \pm 0.19 \pm 0.10$
2	0.092	$-0.54 \pm 1.25 \pm 0.24 \pm 0.10$	0.088	$-0.15 \pm 0.89 \pm 0.14 \pm 0.10$
3	0.156	$-0.78 \pm 1.13 \pm 0.24 \pm 0.10$	0.156	$-1.95 \pm 0.75 \pm 0.16 \pm 0.10$
4	0.208	$-0.04 \pm 0.78 \pm 0.29 \pm 0.10$	0.202	$-0.22 \pm 0.50 \pm 0.17 \pm 0.10$
5	0.094	$-0.78 \pm 0.70 \pm 0.22 \pm 0.10$	0.095	$-0.83 \pm 0.45 \pm 0.14 \pm 0.10$
6	0.144	$-0.82 \pm 0.80 \pm 0.22 \pm 0.10$	0.151	$-0.61 \pm 0.52 \pm 0.14 \pm 0.10$
7	0.064	$-0.04 \pm 0.79 \pm 0.28 \pm 0.10$	0.068	$-0.17 \pm 0.51 \pm 0.17 \pm 0.10$
8	0.028	$-2.24 \pm 0.92 \pm 0.23 \pm 0.10$	0.030	$-0.19 \pm 0.60 \pm 0.15 \pm 0.10$
9	0.032	$+0.23 \pm 1.59 \pm 0.23 \pm 0.10$	0.038	$-1.33 \pm 1.05 \pm 0.14 \pm 0.10$
Integrated		$-0.41 \pm 0.42 \pm 0.26 \pm 0.10$		$-0.53 \pm 0.26 \pm 0.16 \pm 0.10$

The measured $\mathcal{A}_{\rm prod}(B^+)$ values for each kinematic bin are listed in Table V for both center-of-mass energies. They are shown as a function of rapidity for the three $p_{\rm T}$ ranges in Fig. 4. Samples of simulated $B^{\pm}$ decays are produced using PYTHIA 8 [20,21] with a specific LHCb configuration [22] and are used to determine the weights that are assigned to each of the nine bins, such that the sum corresponds to the asymmetry integrated over the full fiducial region covering $2 < p_{\rm T} < 30$ GeV/c and $2.1 < y < 4.5$. These weights are listed in Table V. The integrated asymmetries, which are also reported in Table V, are

$$\mathcal{A}_{\rm prod}(B^+, \sqrt{s} = 7\ {\rm TeV}) = (-0.41 \pm 0.49 \pm 0.10) \times 10^{-2},$$
$$\mathcal{A}_{\rm prod}(B^+, \sqrt{s} = 8\ {\rm TeV}) = (-0.53 \pm 0.31 \pm 0.10) \times 10^{-2},$$

where the first uncertainty is statistical and includes contributions from $\mathcal{A}^{D\pi}_{\rm raw}$ and the detection asymmetry corrections which are inherently statistical in nature. The second uncertainty is systematic. Several cross-checks are performed. The measured value of $\mathcal{A}_{\rm prod}(B^+)$ is found to have no statistically significant dependence on the B^+ decay time or kaon momentum. Statistically compatible results are obtained for the two magnet polarities.

VI. MEASUREMENT OF $\mathcal{A}_{CP}(B^+ \to J/\psi K^+)$

The value of $\mathcal{A}_{CP}(B^+ \to J/\psi K^+)$ is determined according to

$$\mathcal{A}_{CP}(B^+ \to J/\psi K^+) = \mathcal{A}^{\psi K}_{\rm raw} - \delta\mathcal{A}^{K\pi}_{\rm det} - \mathcal{A}^{D\pi}_{\rm raw} + \mathcal{A}^{D\pi}_{CP}, \quad (7)$$

where $\mathcal{A}^{\psi K}_{\rm raw}$ is the raw asymmetry of $B^{\pm} \to J/\psi K^{\pm}$ decays and $\delta\mathcal{A}^{K\pi}_{\rm det}$ corrects for the different detection asymmetries of the two decay modes. The two final states differ by the transformation of a $\pi^+\pi^-$ pair to a $\mu^+\mu^-$ pair, where the only significant contribution to the difference between the overall detection asymmetries arises from the charged kaon asymmetry. The method used to determine $\mathcal{A}^{K\pi}_{\rm det}$, as described in the previous section, is applied to the $J/\psi K^+$ final state by considering the muon with opposite charge to the kaon as a pion. The difference between this and the corresponding asymmetry for the $B^+ \to \bar{D}^0\pi^+$ mode is defined as $\delta\mathcal{A}^{K\pi}_{\rm det} = \mathcal{A}^{K\pi}_{\rm det}(B \to J/\psi K) - \mathcal{A}^{K\pi}_{\rm det}(B \to \bar{D}^0\pi)$. The uncertainties are cancelled to a large degree in this difference.

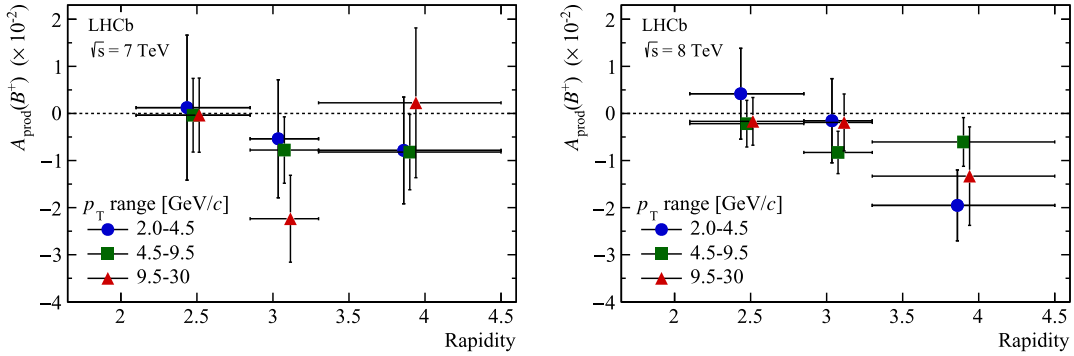

FIG. 4. The measured $\mathcal{A}_{\rm prod}(B^+)$ as a function of rapidity of the B meson in three bins of $p_{\rm T}$. The ranges of $p_{\rm T}$ are indicated in the legends. The left- and right-hand figures correspond to 7 and 8 TeV center-of-mass energies, respectively.

TABLE VI. Residual differences $\delta\mathcal{A}_{\rm det}^{K\pi}$, measured in each bin of B kinematics. These are the effective values after summing over center-of-mass energies and averaging over the two $\bar{D}^0$ decay modes.

Bin	$\delta\mathcal{A}_{\rm det}^{K\pi}$ $(\times 10^{-2})$
1	0.15 ± 0.04
2	0.22 ± 0.03
3	0.24 ± 0.05
4	0.26 ± 0.02
5	0.29 ± 0.02
6	0.21 ± 0.02
7	0.27 ± 0.02
8	0.23 ± 0.01
9	0.05 ± 0.02

Table VI lists the values of $\delta\mathcal{A}_{\rm det}^{K\pi}$ for each kinematic bin. The values of $\delta\mathcal{A}_{\rm det}^{K\pi}$ are positive, since the kaons in the $J/\psi K^+$ decays tend to have higher momenta than those in the $B^+ \to \bar{D}^0\pi^+$ decays. A further asymmetry could result from differences between the kinematic distributions of the pion in the $B^+ \to \bar{D}^0\pi^+$ decay compared to the μ^+ in the $J/\psi K^+$ decay, but this is estimated to be negligibly small.

The values of $\mathcal{A}_{\rm raw}^{\psi K}$ in each bin are corrected according to Eq. (7) using measurements of $\mathcal{A}_{\rm raw}^{D\pi}$, $\delta\mathcal{A}_{\rm det}^{K\pi}$, and $\mathcal{A}_{CP}^{D\pi}$ in order to extract $\mathcal{A}_{CP}(B^+ \to J/\psi K^+)$. Gaussian constraints are applied to the values of $\mathcal{A}_{\rm raw}^{D\pi}$ and $\delta\mathcal{A}_{\rm det}^{K\pi}$, such that the statistical uncertainty on these parameters is included in the overall statistical uncertainty for $\mathcal{A}_{CP}(B^+ \to J/\psi K^+)$. A systematic uncertainty of 0.02×10^{-2} is assigned for the use of fixed parameters in the mass fits, while a systematic uncertainty of 0.05×10^{-2} is assigned for the method used to measure $\delta\mathcal{A}_{\rm det}^{K\pi}$. The $\mathcal{A}_{CP}^{D\pi}$ values contribute a systematic uncertainty of 0.04×10^{-2}. The final result is

$$\mathcal{A}_{CP}(B^+ \to J/\psi K^+) = (0.09 \pm 0.27 \pm 0.07) \times 10^{-2},$$

where the first uncertainty is statistical and the second is systematic. By fixing all Gaussian constrained parameters to have zero uncertainty, the contribution from the finite $B^+ \to J/\psi K^+$ statistics is found to be $\pm 0.20 \times 10^{-2}$. This result is consistent with, and improves upon, the current world average value of $\mathcal{A}_{CP}(B^+ \to J/\psi K^+) = (0.3 \pm 0.6)\%$ [4].

VII. SUMMARY AND CONCLUSIONS

The B^+ meson production asymmetry is a crucial input in the measurement of CP asymmetries in B^+ decays. A sample of $B^+ \to \bar{D}^0\pi^+$ decays is used to measure the production asymmetry. The analyzed data set corresponds to integrated luminosities of 1 and 2 fb^{-1} recorded during 2011 and 2012 at proton-proton center-of-mass energies of 7 and 8 TeV, respectively. The production asymmetries are measured in nine bins of transverse momenta and rapidity, covering the region $2 < p_{\rm T} < 30$ GeV/c and $2.1 < y < 4.5$, and separately for the two center-of-mass energies. The measurements are generally consistent with zero asymmetry within typical uncertainties of roughly 10^{-2}, which is in agreement with b -quark hadronization models [1–3]. Integrated over the full $p_{\rm T}$ and y ranges, the production asymmetries are measured to be

$$\mathcal{A}_{\rm prod}(B^+, \sqrt{s} = 7\ {\rm TeV}) = (-0.41 \pm 0.49 \pm 0.10) \times 10^{-2},$$
$$\mathcal{A}_{\rm prod}(B^+, \sqrt{s} = 8\ {\rm TeV}) = (-0.53 \pm 0.31 \pm 0.10) \times 10^{-2},$$

where the first uncertainty accounts for all statistical sources and the second accounts for all systematic sources. A simultaneous study of the $B^+ \to J/\psi K^+$ decay allows a measurement of its CP asymmetry,

$$\mathcal{A}_{CP}(B^+ \to J/\psi K^+) = (0.09 \pm 0.27 \pm 0.07) \times 10^{-2}.$$

ACKNOWLEDGMENTS

We express our gratitude to our colleagues in the CERN accelerator departments for the excellent performance of the LHC. We thank the technical and administrative staff at the LHCb institutes. We acknowledge support from CERN and from the national agencies: CAPES, CNPq, FAPERJ, and FINEP (Brazil); NSFC (China); CNRS/IN2P3 (France); BMBF, DFG, and MPG (Germany); INFN (Italy); FOM and NWO (Netherlands); MNiSW and NCN (Poland); MEN/IFA (Romania); MinES and FASO (Russia); MinECo (Spain); SNSF and SER (Switzerland); NASU (Ukraine); STFC (United Kingdom); NSF (USA). We acknowledge the computing resources that are provided by CERN, IN2P3 (France), KIT and DESY (Germany), INFN (Italy), SURF (Netherlands), PIC (Spain), GridPP (United Kingdom), RRCKI and Yandex LLC (Russia), CSCS (Switzerland), IFIN-HH (Romania), CBPF (Brazil), PL-GRID (Poland), and OSC (USA). We are indebted to the communities behind the multiple open source software packages on which we depend. Individual groups or members have received support from Alexander von Humboldt (AvH) Foundation (Germany), EPLANET, Marie Skłodowska-Curie Actions and ERC (European Union), Conseil Général de Haute-Savoie, Labex ENIGMASS and OCEVU, Région Auvergne (France), RFBR and Yandex LLC (Russia), GVA, XuntaGal and GENCAT (Spain), Herchel Smith Fund, The Royal Society, Royal Commission for the Exhibition of 1851, and the Leverhulme Trust (United Kingdom).

[1] E. Norrbin and T. Sjöstrand, Production and hadronization of heavy quarks, Eur. Phys. J. C **17**, 137 (2000).

[2] E. Norrbin and R. Vogt, Bottom Production Asymmetries at the LHC, arXiv:hep-ph/0003056.

[3] E. Norrbin, Heavy Quark Production Asymmetries, arXiv:hep-ph/9909437.

[4] C. Patrignani *et al.* (Particle Data Group Collaboration), Review of particle physics, Chin. Phys. C **40**, 100001 (2016).

[5] R. Aaij *et al.* (LHCb Collaboration), Measurement of the $D_s^+ - D_s^-$ production asymmetry in 7 TeV pp collisions, Phys. Lett. B **713**, 186 (2012).

[6] R. Aaij *et al.* (LHCb Collaboration), Measurement of the $D^{\pm}$ production asymmetry in 7 TeV pp collisions, Phys. Lett. B **718**, 902 (2013).

[7] R. Aaij *et al.* (LHCb Collaboration), Measurement of the $B_s^0 - \bar{B}_s^0$ and $B^0 - \bar{B}^0$ production asymmetries in pp collisions at $\sqrt{s} = 7$ TeV, Phys. Lett. B **739**, 218 (2014).

[8] R. Aaij *et al.* (LHCb Collaboration), Measurement of the Semileptonic CP Asymmetry in $B^0 - \bar{B}^0$ Mixing, Phys. Rev. Lett. **114**, 041601 (2015).

[9] A. A. Alves, Jr. *et al.* (LHCb Collaboration), The LHCb detector at the LHC, JINST **3**, S08005 (2008).

[10] R. Aaij *et al.* (LHCb Collaboration), LHCb detector performance, Int. J. Mod. Phys. A **30**, 1530022 (2015).

[11] R. Aaij *et al.*, The LHCb trigger and its performance in 2011, JINST **8**, P04022 (2013).

[12] R. Aaij *et al.* (LHCb Collaboration), Measurement of CP observables in $B^{\pm} \to DK^{\pm}$ and $B^{\pm} \to D\pi^{\pm}$ with two- and four-body D decays, Phys. Lett. B **760**, 117 (2016).

[13] L. Breiman, J. H. Friedman, R. A. Olshen, and C. J. Stone, *Classification and Regression Trees* (Wadsworth International Group, Belmont, CA, 1984).

[14] B. P. Roe, H.-J. Yang, J. Zhu, Y. Liu, I. Stancu, and G. McGregor, Boosted decision trees as an alternative to artificial neural networks for particle identification, Nucl. Instrum. Methods Phys. Res., Sect. A **543**, 577 (2005).

[15] L. Anderlini *et al.*, The PIDCalib package, Report No. LHCb-PUB-2016-021.

[16] R. Aaij *et al.* (LHCb Collaboration), Measurement of the track reconstruction efficiency at LHCb, JINST **10**, P02007 (2015).

[17] N. Cabibbo, Unitary Symmetry and Leptonic Decays, Phys. Rev. Lett. **10**, 531 (1963).

[18] M. Kobayashi and T. Maskawa, CP violation in the renormalizable theory of weak interaction, Prog. Theor. Phys. **49**, 652 (1973).

[19] R. Aaij *et al.* (LHCb Collaboration), Measurement of the CKM angle γ from a combination of LHCb results, J. High Energy Phys. 12 (2016) 087.

[20] T. Sjöstrand, S. Mrenna, and P. Z. Skands, A brief introduction to PYTHIA 8.1, Comput. Phys. Commun. **178**, 852 (2008).

[21] T. Sjöstrand, S. Mrenna, and P. Skands, PYTHIA 6.4 physics and manual, J. High Energy Phys. 05 (2006) 026.

[22] I. Belyaev *et al.*, Handling of the generation of primary events in Gauss, the LHCb simulation framework, J. Phys. Conf. Ser. **331**, 032047 (2011).

R. Aaij,[40] B. Adeva,[39] M. Adinolfi,[48] Z. Ajaltouni,[5] S. Akar,[59] J. Albrecht,[10] F. Alessio,[40] M. Alexander,[53] S. Ali,[43] G. Alkhazov,[31] P. Alvarez Cartelle,[55] A. A. Alves Jr.,[59] S. Amato,[2] S. Amerio,[23] Y. Amhis,[7] L. An,[3] L. Anderlini,[18] G. Andreassi,[41] M. Andreotti,[17,a] J. E. Andrews,[60] R. B. Appleby,[56] F. Archilli,[43] P. d'Argent,[12] J. Arnau Romeu,[6] A. Artamonov,[37] M. Artuso,[61] E. Aslanides,[6] G. Auriemma,[26] M. Baalouch,[5] I. Babuschkin,[56] S. Bachmann,[12] J. J. Back,[50] A. Badalov,[38] C. Baesso,[62] S. Baker,[55] V. Balagura,[7,b] W. Baldini,[17] R. J. Barlow,[56] C. Barschel,[40] S. Barsuk,[7] W. Barter,[56] F. Baryshnikov,[32] M. Baszczyk,[27] V. Batozskaya,[29] B. Batsukh,[61] V. Battista,[41] A. Bay,[41] L. Beaucourt,[4] J. Beddow,[53] F. Bedeschi,[24] I. Bediaga,[1] L. J. Bel,[43] V. Bellee,[41] N. Belloli,[21,c] K. Belous,[37] I. Belyaev,[32] E. Ben-Haim,[8] G. Bencivenni,[19] S. Benson,[43] A. Berezhnoy,[33] R. Bernet,[42] A. Bertolin,[23] C. Betancourt,[42] F. Betti,[15] M.-O. Bettler,[40] M. van Beuzekom,[43] Ia. Bezshyiko,[42] S. Bifani,[47] P. Billoir,[8] T. Bird,[56] A. Birnkraut,[10] A. Bitadze,[56] A. Bizzeti,[18,d] T. Blake,[50] F. Blanc,[41] J. Blouw,[11,†] S. Blusk,[61] V. Bocci,[26] T. Boettcher,[58] A. Bondar,[36,e] N. Bondar,[31,40] W. Bonivento,[16] I. Bordyuzhin,[32] A. Borgheresi,[21,c] S. Borghi,[56] M. Borisyak,[35] M. Borsato,[39] F. Bossu,[7] M. Boubdir,[9] T. J. V. Bowcock,[54] E. Bowen,[42] C. Bozzi,[17,40] S. Braun,[12] M. Britsch,[12] T. Britton,[61] J. Brodzicka,[56] E. Buchanan,[48] C. Burr,[56] A. Bursche,[2] J. Buytaert,[40] S. Cadeddu,[16] R. Calabrese,[17,a] M. Calvi,[21,c] M. Calvo Gomez,[38,f] A. Camboni,[38] P. Campana,[19] D. H. Campora Perez,[40] L. Capriotti,[56] A. Carbone,[15,g] G. Carboni,[25,h] R. Cardinale,[20,i] A. Cardini,[16] P. Carniti,[21,c] L. Carson,[52] K. Carvalho Akiba,[2] G. Casse,[54] L. Cassina,[21,c] L. Castillo Garcia,[41] M. Cattaneo,[40] G. Cavallero,[20] R. Cenci,[24,j] D. Chamont,[7] M. Charles,[8] Ph. Charpentier,[40] G. Chatzikonstantinidis,[47] M. Chefdeville,[4] S. Chen,[56] S.-F. Cheung,[57] V. Chobanova,[39] M. Chrzaszcz,[42,27] X. Cid Vidal,[39] G. Ciezarek,[43] P. E. L. Clarke,[52] M. Clemencic,[40] H. V. Cliff,[49] J. Closier,[40] V. Coco,[59] J. Cogan,[6] E. Cogneras,[5] V. Cogoni,[16,40,k] L. Cojocariu,[30] G. Collazuol,[23,l] P. Collins,[40] A. Comerma-Montells,[12] A. Contu,[40] A. Cook,[48] G. Coombs,[40] S. Coquereau,[38] G. Corti,[40] M. Corvo,[17,a] C. M. Costa Sobral,[50] B. Couturier,[40] G. A. Cowan,[52] D. C. Craik,[52] A. Crocombe,[50] M. Cruz Torres,[62] S. Cunliffe,[55] R. Currie,[55] C. D'Ambrosio,[40] F. Da Cunha Marinho,[2] E. Dall'Occo,[43] J. Dalseno,[48] P. N. Y. David,[43] A. Davis,[3] K. De Bruyn,[6] S. De Capua,[56] M. De Cian,[12] J. M. De Miranda,[1] L. De Paula,[2] M. De Serio,[14,m] P. De Simone,[19] C. T. Dean,[53] D. Decamp,[4] M. Deckenhoff,[10] L. Del Buono,[8] M. Demmer,[10]

A. Dendek,[28] D. Derkach,[35] O. Deschamps,[5] F. Dettori,[40] B. Dey,[22] A. Di Canto,[40] H. Dijkstra,[40] F. Dordei,[40] M. Dorigo,[41] A. Dosil Suárez,[39] A. Dovbnya,[45] K. Dreimanis,[54] L. Dufour,[43] G. Dujany,[56] K. Dungs,[40] P. Durante,[40] R. Dzhelyadin,[37] A. Dziurda,[40] A. Dzyuba,[31] N. Déléage,[4] S. Easo,[51] M. Ebert,[52] U. Egede,[55] V. Egorychev,[32] S. Eidelman,[36,e] S. Eisenhardt,[52] U. Eitschberger,[10] R. Ekelhof,[10] L. Eklund,[53] S. Ely,[61] S. Esen,[12] H. M. Evans,[49] T. Evans,[57] A. Falabella,[15] N. Farley,[47] S. Farry,[54] R. Fay,[54] D. Fazzini,[21,c] D. Ferguson,[52] A. Fernandez Prieto,[39] F. Ferrari,[15,40] F. Ferreira Rodrigues,[2] M. Ferro-Luzzi,[40] S. Filippov,[34] R. A. Fini,[14] M. Fiore,[17,a] M. Fiorini,[17,a] M. Firlej,[28] C. Fitzpatrick,[41] T. Fiutowski,[28] F. Fleuret,[7,n] K. Fohl,[40] M. Fontana,[16,40] F. Fontanelli,[20,i] D. C. Forshaw,[61] R. Forty,[40] V. Franco Lima,[54] M. Frank,[40] C. Frei,[40] J. Fu,[22,o] W. Funk,[40] E. Furfaro,[25,h] C. Färber,[40] A. Gallas Torreira,[39] D. Galli,[15,g] S. Gallorini,[23] S. Gambetta,[52] M. Gandelman,[2] P. Gandini,[57] Y. Gao,[3] L. M. Garcia Martin,[69] J. García Pardiñas,[39] J. Garra Tico,[49] L. Garrido,[38] P. J. Garsed,[49] D. Gascon,[38] C. Gaspar,[40] L. Gavardi,[10] G. Gazzoni,[5] D. Gerick,[12] E. Gersabeck,[12] M. Gersabeck,[56] T. Gershon,[50] Ph. Ghez,[4] S. Gianì,[41] V. Gibson,[49] O. G. Girard,[41] L. Giubega,[30] K. Gizdov,[52] V. V. Gligorov,[8] D. Golubkov,[32] A. Golutvin,[55,40] A. Gomes,[1,p] I. V. Gorelov,[33] C. Gotti,[21,c] R. Graciani Diaz,[38] L. A. Granado Cardoso,[40] E. Graugés,[38] E. Graverini,[42] G. Graziani,[18] A. Grecu,[30] P. Griffith,[47] L. Grillo,[21,40,c] B. R. Gruberg Cazon,[57] O. Grünberg,[67] E. Gushchin,[34] Yu. Guz,[37] T. Gys,[40] C. Göbel,[62] T. Hadavizadeh,[57] C. Hadjivasiliou,[5] G. Haefeli,[41] C. Haen,[40] S. C. Haines,[49] B. Hamilton,[60] X. Han,[12] S. Hansmann-Menzemer,[12] N. Harnew,[57] S. T. Harnew,[48] J. Harrison,[56] M. Hatch,[40] J. He,[63] T. Head,[41] A. Heister,[9] K. Hennessy,[54] P. Henrard,[5] L. Henry,[8] E. van Herwijnen,[40] M. Heß,[67] A. Hicheur,[2] D. Hill,[57] C. Hombach,[56] H. Hopchev,[41] W. Hulsbergen,[43] T. Humair,[55] M. Hushchyn,[35] D. Hutchcroft,[54] M. Idzik,[28] P. Ilten,[58] R. Jacobsson,[40] A. Jaeger,[12] J. Jalocha,[57] E. Jans,[43] A. Jawahery,[60] F. Jiang,[3] M. John,[57] D. Johnson,[40] C. R. Jones,[49] C. Joram,[40] B. Jost,[40] N. Jurik,[57] S. Kandybei,[45] M. Karacson,[40] J. M. Kariuki,[48] S. Karodia,[53] M. Kecke,[12] M. Kelsey,[61] M. Kenzie,[49] T. Ketel,[44] E. Khairullin,[35] B. Khanji,[12] C. Khurewathanakul,[41] T. Kirn,[9] S. Klaver,[56] K. Klimaszewski,[29] S. Koliiev,[46] M. Kolpin,[12] I. Komarov,[41] R. F. Koopman,[44] P. Koppenburg,[43] A. Kosmyntseva,[32] A. Kozachuk,[33] M. Kozeiha,[5] L. Kravchuk,[34] K. Kreplin,[12] M. Kreps,[50] P. Krokovny,[36,e] F. Kruse,[10] W. Krzemien,[29] W. Kucewicz,[27,q] M. Kucharczyk,[27] V. Kudryavtsev,[36,e] A. K. Kuonen,[41] K. Kurek,[29] T. Kvaratskheliya,[32,40] D. Lacarrere,[40] G. Lafferty,[56] A. Lai,[16] G. Lanfranchi,[19] C. Langenbruch,[9] T. Latham,[50] C. Lazzeroni,[47] R. Le Gac,[6] J. van Leerdam,[43] A. Leflat,[33,40] J. Lefrançois,[7] R. Lefèvre,[5] F. Lemaitre,[40] E. Lemos Cid,[39] O. Leroy,[6] T. Lesiak,[27] B. Leverington,[12] T. Li,[3] Y. Li,[7] T. Likhomanenko,[35,68] R. Lindner,[40] C. Linn,[40] F. Lionetto,[42] X. Liu,[3] D. Loh,[50] I. Longstaff,[53] J. H. Lopes,[2] D. Lucchesi,[23,l] M. Lucio Martinez,[39] H. Luo,[52] A. Lupato,[23] E. Luppi,[17,a] O. Lupton,[40] A. Lusiani,[24] X. Lyu,[63] F. Machefert,[7] F. Maciuc,[30] O. Maev,[31] K. Maguire,[56] S. Malde,[57] A. Malinin,[68] T. Maltsev,[36] G. Manca,[16,k] G. Mancinelli,[6] P. Manning,[61] J. Maratas,[5,r] J. F. Marchand,[4] U. Marconi,[15] C. Marin Benito,[38] M. Marinangeli,[41] P. Marino,[24,j] J. Marks,[12] G. Martellotti,[26] M. Martin,[6] M. Martinelli,[41] D. Martinez Santos,[39] F. Martinez Vidal,[69] D. Martins Tostes,[2] L. M. Massacrier,[7] A. Massafferri,[1] R. Matev,[40] A. Mathad,[50] Z. Mathe,[40] C. Matteuzzi,[21] A. Mauri,[42] E. Maurice,[7,n] B. Maurin,[41] A. Mazurov,[47] M. McCann,[55,40] A. McNab,[56] R. McNulty,[13] B. Meadows,[59] F. Meier,[10] M. Meissner,[12] D. Melnychuk,[29] M. Merk,[43] A. Merli,[22,o] E. Michielin,[23] D. A. Milanes,[66] M.-N. Minard,[4] D. S. Mitzel,[12] A. Mogini,[8] J. Molina Rodriguez,[1] I. A. Monroy,[66] S. Monteil,[5] M. Morandin,[23] P. Morawski,[28] A. Mordà,[6] M. J. Morello,[24,j] O. Morgunova,[68] J. Moron,[28] A. B. Morris,[52] R. Mountain,[61] F. Muheim,[52] M. Mulder,[43] M. Mussini,[15] D. Müller,[56] J. Müller,[10] K. Müller,[42] V. Müller,[10] P. Naik,[48] T. Nakada,[41] R. Nandakumar,[51] A. Nandi,[57] I. Nasteva,[2] M. Needham,[52] N. Neri,[22] S. Neubert,[12] N. Neufeld,[40] M. Neuner,[12] T. D. Nguyen,[41] C. Nguyen-Mau,[41,s] S. Nieswand,[9] R. Niet,[10] N. Nikitin,[33] T. Nikodem,[12] A. Nogay,[68] A. Novoselov,[37] D. P. O'Hanlon,[50] A. Oblakowska-Mucha,[28] V. Obraztsov,[37] S. Ogilvy,[19] R. Oldeman,[16,k] C. J. G. Onderwater,[70] J. M. Otalora Goicochea,[2] A. Otto,[40] P. Owen,[42] A. Oyanguren,[69] P. R. Pais,[41] A. Palano,[14,m] F. Palombo,[22,o] M. Palutan,[19] A. Papanestis,[51] M. Pappagallo,[14,m] L. L. Pappalardo,[17,a] W. Parker,[60] C. Parkes,[56] G. Passaleva,[18] A. Pastore,[14,m] G. D. Patel,[54] M. Patel,[55] C. Patrignani,[15,g] A. Pearce,[40] A. Pellegrino,[43] G. Penso,[26] M. Pepe Altarelli,[40] S. Perazzini,[40] P. Perret,[5] L. Pescatore,[47] K. Petridis,[48] A. Petrolini,[20,i] A. Petrov,[68] M. Petruzzo,[22,o] E. Picatoste Olloqui,[38] B. Pietrzyk,[4] M. Pikies,[27] D. Pinci,[26] A. Pistone,[20] A. Piucci,[12] V. Placinta,[30] S. Playfer,[52] M. Plo Casasus,[39] T. Poikela,[40] F. Polci,[8] A. Poluektov,[50,36] I. Polyakov,[61] E. Polycarpo,[2] G. J. Pomery,[48] A. Popov,[37] D. Popov,[11,40] B. Popovici,[30] S. Poslavskii,[37] C. Potterat,[2] E. Price,[48] J. D. Price,[54] J. Prisciandaro,[39,40] A. Pritchard,[54] C. Prouve,[48] V. Pugatch,[46] A. Puig Navarro,[42] G. Punzi,[24,t] W. Qian,[50] R. Quagliani,[7,48] B. Rachwal,[27] J. H. Rademacker,[48] M. Rama,[24] M. Ramos Pernas,[39] M. S. Rangel,[2] I. Raniuk,[45] F. Ratnikov,[35] G. Raven,[44] F. Redi,[55] S. Reichert,[10] A. C. dos Reis,[1] C. Remon Alepuz,[69] V. Renaudin,[7] S. Ricciardi,[51] S. Richards,[48] M. Rihl,[40] K. Rinnert,[54] V. Rives Molina,[38] P. Robbe,[7,40] A. B. Rodrigues,[1] E. Rodrigues,[59] J. A. Rodriguez Lopez,[66] P. Rodriguez Perez,[56,†] A. Rogozhnikov,[35]

S. Roiser,[40] A. Rollings,[57] V. Romanovskiy,[37] A. Romero Vidal,[39] J. W. Ronayne,[13] M. Rotondo,[19] M. S. Rudolph,[61] T. Ruf,[40] P. Ruiz Valls,[69] J. J. Saborido Silva,[39] E. Sadykhov,[32] N. Sagidova,[31] B. Saitta,[16,k] V. Salustino Guimaraes,[1] C. Sanchez Mayordomo,[69] B. Sanmartin Sedes,[39] R. Santacesaria,[26] C. Santamarina Rios,[39] M. Santimaria,[19] E. Santovetti,[25,h] A. Sarti,[19,u] C. Satriano,[26,v] A. Satta,[25] D. M. Saunders,[48] D. Savrina,[32,33] S. Schael,[9] M. Schellenberg,[10] M. Schiller,[53] H. Schindler,[40] M. Schlupp,[10] M. Schmelling,[11] T. Schmelzer,[10] B. Schmidt,[40] O. Schneider,[41] A. Schopper,[40] K. Schubert,[10] M. Schubiger,[41] M.-H. Schune,[7] R. Schwemmer,[40] B. Sciascia,[19] A. Sciubba,[26,u] A. Semennikov,[32] A. Sergi,[47] N. Serra,[42] J. Serrano,[6] L. Sestini,[23] P. Seyfert,[21] M. Shapkin,[37] I. Shapoval,[45] Y. Shcheglov,[31] T. Shears,[54] L. Shekhtman,[36,e] V. Shevchenko,[68] B. G. Siddi,[17,40] R. Silva Coutinho,[42] L. Silva de Oliveira,[2] G. Simi,[23,l] S. Simone,[14,m] M. Sirendi,[49] N. Skidmore,[48] T. Skwarnicki,[61] E. Smith,[55] I. T. Smith,[52] J. Smith,[49] M. Smith,[55] H. Snoek,[43] l. Soares Lavra,[1] M. D. Sokoloff,[59] F. J. P. Soler,[53] B. Souza De Paula,[2] B. Spaan,[10] P. Spradlin,[53] S. Sridharan,[40] F. Stagni,[40] M. Stahl,[12] S. Stahl,[40] P. Stefko,[41] S. Stefkova,[55] O. Steinkamp,[42] S. Stemmle,[12] O. Stenyakin,[37] H. Stevens,[10] S. Stevenson,[57] S. Stoica,[30] S. Stone,[61] B. Storaci,[42] S. Stracka,[24,t] M. Straticiuc,[30] U. Straumann,[42] L. Sun,[64] W. Sutcliffe,[55] K. Swientek,[28] V. Syropoulos,[44] M. Szczekowski,[29] T. Szumlak,[28] S. T'Jampens,[4] A. Tayduganov,[6] T. Tekampe,[10] G. Tellarini,[17,a] F. Teubert,[40] E. Thomas,[40] J. van Tilburg,[43] M. J. Tilley,[55] V. Tisserand,[4] M. Tobin,[41] S. Tolk,[49] L. Tomassetti,[17,a] D. Tonelli,[40] S. Topp-Joergensen,[57] F. Toriello,[61] E. Tournefier,[4] S. Tourneur,[41] K. Trabelsi,[41] M. Traill,[53] M. T. Tran,[41] M. Tresch,[42] A. Trisovic,[40] A. Tsaregorodtsev,[6] P. Tsopelas,[43] A. Tully,[49] N. Tuning,[43] A. Ukleja,[29] A. Ustyuzhanin,[35] U. Uwer,[12] C. Vacca,[16,k] V. Vagnoni,[15,40] A. Valassi,[40] S. Valat,[40] G. Valenti,[15] R. Vazquez Gomez,[19] P. Vazquez Regueiro,[39] S. Vecchi,[17] M. van Veghel,[43] J. J. Velthuis,[48] M. Veltri,[18,w] G. Veneziano,[57] A. Venkateswaran,[61] M. Vernet,[5] M. Vesterinen,[12] J. V. Viana Barbosa,[40] B. Viaud,[7] D. Vieira,[63] M. Vieites Diaz,[39] H. Viemann,[67] X. Vilasis-Cardona,[38,f] M. Vitti,[49] V. Volkov,[33] A. Vollhardt,[42] B. Voneki,[40] A. Vorobyev,[31] V. Vorobyev,[36,e] C. Voß,[9] J. A. de Vries,[43] C. Vázquez Sierra,[39] R. Waldi,[67] C. Wallace,[50] R. Wallace,[13] J. Walsh,[24] J. Wang,[61] D. R. Ward,[49] H. M. Wark,[54] N. K. Watson,[47] D. Websdale,[55] A. Weiden,[42] M. Whitehead,[40] J. Wicht,[50] G. Wilkinson,[57,40] M. Wilkinson,[61] M. Williams,[40] M. P. Williams,[47] M. Williams,[58] T. Williams,[47] F. F. Wilson,[51] J. Wimberley,[60] J. Wishahi,[10] W. Wislicki,[29] M. Witek,[27] G. Wormser,[7] S. A. Wotton,[49] K. Wraight,[53] K. Wyllie,[40] Y. Xie,[65] Z. Xing,[61] Z. Xu,[4] Z. Yang,[3] Y. Yao,[61] H. Yin,[65] J. Yu,[65] X. Yuan,[36,e] O. Yushchenko,[37] K. A. Zarebski,[47] M. Zavertyaev,[11,b] L. Zhang,[3] Y. Zhang,[7] Y. Zhang,[63] A. Zhelezov,[12] Y. Zheng,[63] X. Zhu,[3] V. Zhukov,[33] and S. Zucchelli[15]

(LHCb Collaboration)

[1]*Centro Brasileiro de Pesquisas Físicas (CBPF), Rio de Janeiro, Brazil*
[2]*Universidade Federal do Rio de Janeiro (UFRJ), Rio de Janeiro, Brazil*
[3]*Center for High Energy Physics, Tsinghua University, Beijing, China*
[4]*LAPP, Université Savoie Mont-Blanc, CNRS/IN2P3, Annecy-Le-Vieux, France*
[5]*Clermont Université, Université Blaise Pascal, CNRS/IN2P3, LPC, Clermont-Ferrand, France*
[6]*CPPM, Aix-Marseille Université, CNRS/IN2P3, Marseille, France*
[7]*LAL, Université Paris-Sud, CNRS/IN2P3, Orsay, France*
[8]*LPNHE, Université Pierre et Marie Curie, Université Paris Diderot, CNRS/IN2P3, Paris, France*
[9]*I. Physikalisches Institut, RWTH Aachen University, Aachen, Germany*
[10]*Fakultät Physik, Technische Universität Dortmund, Dortmund, Germany*
[11]*Max-Planck-Institut für Kernphysik (MPIK), Heidelberg, Germany*
[12]*Physikalisches Institut, Ruprecht-Karls-Universität Heidelberg, Heidelberg, Germany*
[13]*School of Physics, University College Dublin, Dublin, Ireland*
[14]*Sezione INFN di Bari, Bari, Italy*
[15]*Sezione INFN di Bologna, Bologna, Italy*
[16]*Sezione INFN di Cagliari, Cagliari, Italy*
[17]*Sezione INFN di Ferrara, Ferrara, Italy*
[18]*Sezione INFN di Firenze, Firenze, Italy*
[19]*Laboratori Nazionali dell'INFN di Frascati, Frascati, Italy*
[20]*Sezione INFN di Genova, Genova, Italy*
[21]*Sezione INFN di Milano Bicocca, Milano, Italy*
[22]*Sezione INFN di Milano, Milano, Italy*
[23]*Sezione INFN di Padova, Padova, Italy*
[24]*Sezione INFN di Pisa, Pisa, Italy*
[25]*Sezione INFN di Roma Tor Vergata, Roma, Italy*

[26]*Sezione INFN di Roma La Sapienza, Roma, Italy*
[27]*Henryk Niewodniczanski Institute of Nuclear Physics Polish Academy of Sciences, Kraków, Poland*
[28]*AGH - University of Science and Technology, Faculty of Physics and Applied Computer Science, Kraków, Poland*
[29]*National Center for Nuclear Research (NCBJ), Warsaw, Poland*
[30]*Horia Hulubei National Institute of Physics and Nuclear Engineering, Bucharest-Magurele, Romania*
[31]*Petersburg Nuclear Physics Institute (PNPI), Gatchina, Russia*
[32]*Institute of Theoretical and Experimental Physics (ITEP), Moscow, Russia*
[33]*Institute of Nuclear Physics, Moscow State University (SINP MSU), Moscow, Russia*
[34]*Institute for Nuclear Research of the Russian Academy of Sciences (INR RAN), Moscow, Russia*
[35]*Yandex School of Data Analysis, Moscow, Russia*
[36]*Budker Institute of Nuclear Physics (SB RAS), Novosibirsk, Russia*
[37]*Institute for High Energy Physics (IHEP), Protvino, Russia*
[38]*ICCUB, Universitat de Barcelona, Barcelona, Spain*
[39]*Universidad de Santiago de Compostela, Santiago de Compostela, Spain*
[40]*European Organization for Nuclear Research (CERN), Geneva, Switzerland*
[41]*Institute of Physics, Ecole Polytechnique Fédérale de Lausanne (EPFL), Lausanne, Switzerland*
[42]*Physik-Institut, Universität Zürich, Zürich, Switzerland*
[43]*Nikhef National Institute for Subatomic Physics, Amsterdam, Netherlands*
[44]*Nikhef National Institute for Subatomic Physics and VU University Amsterdam, Amsterdam, Netherlands*
[45]*NSC Kharkiv Institute of Physics and Technology (NSC KIPT), Kharkiv, Ukraine*
[46]*Institute for Nuclear Research of the National Academy of Sciences (KINR), Kyiv, Ukraine*
[47]*University of Birmingham, Birmingham, United Kingdom*
[48]*H.H. Wills Physics Laboratory, University of Bristol, Bristol, United Kingdom*
[49]*Cavendish Laboratory, University of Cambridge, Cambridge, United Kingdom*
[50]*Department of Physics, University of Warwick, Coventry, United Kingdom*
[51]*STFC Rutherford Appleton Laboratory, Didcot, United Kingdom*
[52]*School of Physics and Astronomy, University of Edinburgh, Edinburgh, United Kingdom*
[53]*School of Physics and Astronomy, University of Glasgow, Glasgow, United Kingdom*
[54]*Oliver Lodge Laboratory, University of Liverpool, Liverpool, United Kingdom*
[55]*Imperial College London, London, United Kingdom*
[56]*School of Physics and Astronomy, University of Manchester, Manchester, United Kingdom*
[57]*Department of Physics, University of Oxford, Oxford, United Kingdom*
[58]*Massachusetts Institute of Technology, Cambridge, Massachusetts, USA*
[59]*University of Cincinnati, Cincinnati, Ohio, USA*
[60]*University of Maryland, College Park, Maryland, USA*
[61]*Syracuse University, Syracuse, New York, USA*
[62]*Pontifícia Universidade Católica do Rio de Janeiro (PUC-Rio), Rio de Janeiro, Brazil (associated with Institution Universidade Federal do Rio de Janeiro (UFRJ), Rio de Janeiro, Brazil)*
[63]*University of Chinese Academy of Sciences, Beijing, China (associated with Institution Center for High Energy Physics, Tsinghua University, Beijing, China)*
[64]*School of Physics and Technology, Wuhan University, Wuhan, China (associated with Institution Center for High Energy Physics, Tsinghua University, Beijing, China)*
[65]*Institute of Particle Physics, Central China Normal University, Wuhan, Hubei, China (associated with Institution Center for High Energy Physics, Tsinghua University, Beijing, China)*
[66]*Departamento de Fisica, Universidad Nacional de Colombia, Bogota, Colombia (associated with Institution LPNHE, Université Pierre et Marie Curie, Université Paris Diderot, CNRS/IN2P3, Paris, France)*
[67]*Institut für Physik, Universität Rostock, Rostock, Germany (associated with Institution Physikalisches Institut, Ruprecht-Karls-Universität Heidelberg, Heidelberg, Germany)*
[68]*National Research Centre Kurchatov Institute, Moscow, Russia (associated with Institution Institute of Theoretical and Experimental Physics (ITEP), Moscow, Russia)*
[69]*Instituto de Fisica Corpuscular, Centro Mixto Universidad de Valencia - CSIC, Valencia, Spain (associated with Institution ICCUB, Universitat de Barcelona, Barcelona, Spain)*
[70]*Van Swinderen Institute, University of Groningen, Groningen, Netherlands (associated with Institution Nikhef National Institute for Subatomic Physics, Amsterdam, Netherlands)*

[†]Deceased.
[a]Also at Università di Ferrara, Ferrara, Italy.

[b]Also at P.N. Lebedev Physical Institute, Russian Academy of Science (LPI RAS), Moscow, Russia.
[c]Also at Università di Milano Bicocca, Milano, Italy.
[d]Also at Università di Modena e Reggio Emilia, Modena, Italy.
[e]Also at Novosibirsk State University, Novosibirsk, Russia.
[f]Also at LIFAELS, La Salle, Universitat Ramon Llull, Barcelona, Spain.
[g]Also at Università di Bologna, Bologna, Italy.
[h]Also at Università di Roma Tor Vergata, Roma, Italy.
[i]Also at Università di Genova, Genova, Italy.
[j]Also at Scuola Normale Superiore, Pisa, Italy.
[k]Also at Università di Cagliari, Cagliari, Italy.
[l]Also at Università di Padova, Padova, Italy.
[m]Also at Università di Bari, Bari, Italy.
[n]Also at Laboratoire Leprince-Ringuet, Palaiseau, France.
[o]Also at Università degli Studi di Milano, Milano, Italy.
[p]Also at Universidade Federal do Triângulo Mineiro (UFTM), Uberaba-MG, Brazil.
[q]Also at AGH - University of Science and Technology, Faculty of Computer Science, Electronics and Telecommunications, Kraków, Poland.
[r]Also at Iligan Institute of Technology (IIT), Iligan, Philippines.
[s]Also at Hanoi University of Science, Hanoi, Viet Nam.
[t]Also at Università di Pisa, Pisa, Italy.
[u]Also at Università di Roma La Sapienza, Roma, Italy.
[v]Also at Università della Basilicata, Potenza, Italy.
[w]Also at Università di Urbino, Urbino, Italy.